The Processing of Observables Made by the HMI Instrument on SDO

J.T. Hoeksema, J. Schou, S. Couvidat, R.S. Bogart, R.I. Bush, T.L. Duvall, Jr., Y. Liu, A.A. Norton, and P.H. Scherrer

The Helioseismic and Magnetic Imager (HMI) acquires sequences of polarized filtergrams of the Sun from which observable quantities are computed. The observables include five line of sight quantities – magnetic field, velocity, continuum intensity, line depth, and line width – as well as Stokes polarization parameters.

The process of turning a set of filtergrams into calibrated measurements is quite involved. Since May 2010 the streams of data from HMI's two cameras have been treated separately. The frame list for the Doppler camera repeats every 45 seconds and the images are combined to determine the line-of-sight observables. The Vector camera sequence measures additional polarizations and so requires 135s; images from ten vector sequences are averaged every 720s to determine the four Stokes polarization parameters at each of six wavelengths, as well as the LoS observables.

A variety of calibration corrections are made to the Level-1 filtergrams to account for distortion, image motion and alignment, polarization, wavelength and intensity irregularities, camera issues, solar rotation, and other effects. Residual random variations in the final observables are consistent with photon noise levels, but systematic errors remain that have not been fully corrected. Of particular concern are those associated with the velocity of the instrument relative to the Sun due to the geosynchronous orbit of the Solar Dynamics Observatory (SDO) spacecraft. This presentation describes the creation of the observables, characterizes the residual errors, and indicates plans for future improvements - including correction for the instrument point spread function. All HMI data are available at http://jsoc.stanford.edu.

Step 1 - Level 1 Filtergrams and Observables

Level-1 filtergrams are 4096**2 CCD images corrected for all of the usual issues - exposure time, dark current, gain, flat field. In addition cosmic rays are identified and corrected (in the definitive data). Various characteristics of the images are also determined, e.g. the center position and wavelength-corrected radius, as well as its overall QUALITY.

The HMI *observables* are calibrated physical quantities computed from a repeating sequence of Level-1 filtergrams observed at specific wavelengths and polarizations. The observables are listed in the **TABLE** along with the random uncertainties that are determined largely by photon noise and choices made during the instrument design. Until April 2016 each of the two HMI cameras provided data for a separate data reduction pipeline. One provides line-of-sight velocity, intensity, and magnetic field samples every 45 seconds. The other also provides additional polarization information necessary to determine the vector field every 135s that is averaged every 720s. Recently HMI has begun combining images from the two cameras and now collects a full set of filtergrams more quickly, every 90s.

Table 1. SDO JSOC Data Series with HMI Observables

Definitive Series Name	NRT Series Name	Photon Noise (Disk Center)	Description
LoS Pipeline			
hmi.V_45s	hmi.V_45s_nrt	17 m s^{-1}	Line-of-sight Velocity
hmi.M_45s	hmi.M_45s_nrt	7 G‡	Line-of-sight Magnetic Field†
hmi.Ic_45s	hmi.Ic_45s_nrt	0.03%	Computed Continuum Intensity
hmi.Lw_45s	hmi.Lw_45s_nrt	1 mÅ	Fe I Line Width
hmi.Ld_45s	hmi.Ld_45s_nrt	0.05%	Fe I Line Depth
Vector Pipeline			
hmi.S_720s	hmi.S_720s_nrt	0.05% for I*	Stokes Polarization Parameters, I Q U V
		0.09% of I for Q U V	
hmi.V_720s	hmi.V_720s_nrt	7 m s^{-1}	Line-of-sight Velocity
hmi.M_720s	hmi.M_720s_nrt	3 G◇	Line-of-sight Magnetic Field†
hmi.Ic_720s	hmi.Ic_720s_nrt	0.01%	Computed Continuum Intensity
hmi.Lw_720s	hmi.Lw_720s_nrt	0.4 mÅ	Fe I Line Width
hmi.Ld_720s	hmi.Ld_720s_nrt	0.02%	Fe I Line Depth

† HMI measures flux density in each pixel. Because a filling factor of 1 is assumed, a flux density of 1 Mx cm^{-2} is equivalent to a field strength of 1 G, and we use the two interchangeably in this report.

‡ Compared with 8.5 G observed in a near disk-center weak-field histogram (Fig. 3 of Liu *et al.*, 2012).

* Photon noise is 26 DN for a typical Intensity of 50K DN/s. Larger noise of 43 DN is expected for Q U & V, which are ten times smaller than I, even in strong-field regions.

◇ Compared with 4 G observed in a near disk-center weak-field histogram (Fig. 3 of Liu *et al.*, 2012).

Step 2 - Image Selection, Correction, and Alignment

The first step is to identify the appropriate images. After filling data gaps and correcting for a small CCD non-linearity, images must be corrected for distortion and interpolated to the same time and location. This involves combining multiple measurements of each wavelength and polarization, even for the 45s data. For convenience we interpolate to times (T_REC) that are evenly spaced when translated to exactly 1 AU. The process requires precise knowledge of the pointing, distortion, and drifts of the two cameras. The cameras differ in roll angle by 0.0837(2) degrees and are drifting together by -0.00020(6) degrees per year. To verify the distortion correction, **FIG 1** shows that the difference between the observed and predicted location of Venus was less than 0.05 pixels during most of the 2012 transit, consistent with the uncertainty in roll at the solar limb of 0.05 pixels.

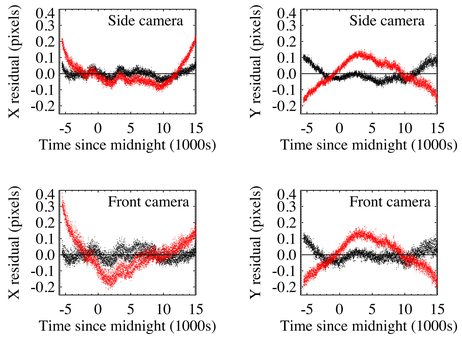

FIG 1: Residuals from the fit of the ephemeris to the measured location of Venus. Red points were determined without the distortion correction. The top panels show results for the "Side" or vector camera and the bottom those for the "Front" camera. The side camera observed only continuum intensity in linear polarization.

Step 3 - Polarization

The HMI optical system introduces polarization that can be measured and modeled. **FIG 2** shows the residual polarization terms from I into Q, U, and V after removing a polynomial fit to the measured demodulation matrix. The figure saturates at 100 ppm. There are changes to the terms of the order 10 ppm over the course of the mission, with annual variations of about the same magnitude. **FIG 3** illustrates a second polarization term for which a correction is made; we call it the Polarization-PSF effect; a blurred I signal appears in Q, U, and V that can be almost completely removed as shown in the bottom panel.

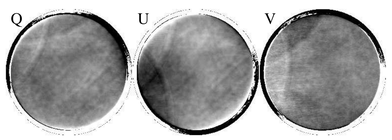

FIG 2: Residual polarization maps from I into Q, U, and V after removing the polynomial fit. The arcs are likely due to an internal reflection in the optical path. These images saturate at +/- 100 ppm.

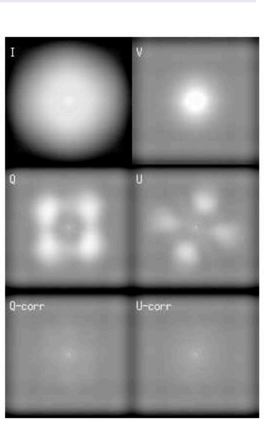

FIG 3: The top four panels show the average power spectra of I Q U V before correcting for the polarization-PSF effect. The bottom two panels show Q and U after correction. The gray scale is logarithmic and saturates at 100 for Q, U, and V and at 100,000 for I.

Step 4 - Wavelength

The HMI filters are not completely uniform and the average wavelength drifts with time. We measure the wavelength sensitivity of the three tunable filter elements (a Lyot element and the wide-band and narrow-band Michelsons) in degrees of phase, corresponding to the angle the linear polarizing element is moved to tune the element through its free spectral range. **FIG 4** shows a colorful representation of the phase maps measured in HMI Calibration Mode on the left. Unfortunately there are intense small-scale fringes in calmode that are introduced by the front window. **FIG 5** shows fits for the correction that must be made to the phase maps (see corrected maps in the left panel of Fig 4). The phase maps allow us to determine the central wavelength for each point in the filtergram images, which is important for the HMI velocity measurement. In addition we know that in observing mode there is an intensity fringe pattern from the front window that appears differently on each of the tunable elements. Currently no correction is made for the resulting I-ripple, but **FIG 6** shows how the I-ripple pattern amplitude has evolved over the course of the mission.

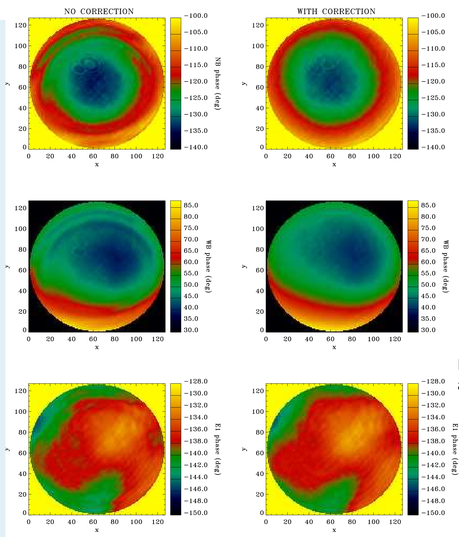

FIG 4: The left column shows the measured wavelength/phase maps for the tunable HMI filter elements. From the top, the Narrow-Band, Wide-Band, and Lyot elements are shown. Units of phase are related to the free spectral range. The right column shows the corrected phase maps after removing the small-scale fringes due to effects of being in calibration mode.

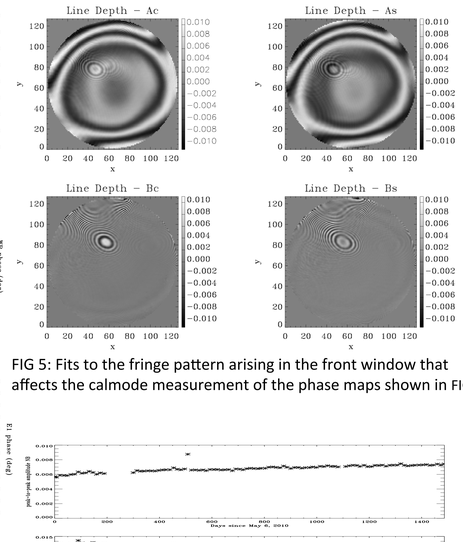

FIG 5: Fits to the fringe pattern arising in the front window that affects the calmode measurement of the phase maps shown in FIG 4.

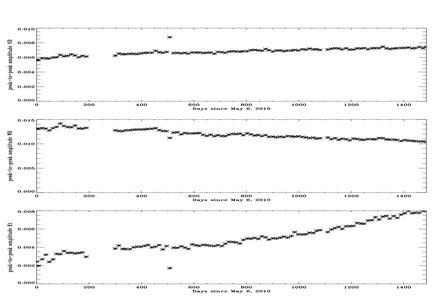

FIG 6: Evolving peak-to-peak amplitude of the I-ripple for the first 1500 days of the SDO mission in the narrow-band, wide-band, and Lyot tunable filter elements (top to bottom).

Step 5 - Determining the Line-of-Sight Observables - the MDI-Method

HMI tunes to just six wavelengths across the spectral line and effectively measures the phase of the resulting signal. The phase gives the line position and line intensity in right and left circular polarization, from which the line-of-sight Doppler velocity and magnetic field strength can be determined, as well as the line depth, line width, and continuum intensity. A similar method was used onboard the SOHO/MDI instrument, hence the name. HMI differs in several ways, in particular the spacing of the wavelengths is different and the line profile moves significantly relative to the filter wavelengths during the daily orbit. Consequently the sensitivity changes with velocity and thus across the disk and with time of day in a way that affects the HMI observables. **FIG 7** show the sensitivity table used to correct the initial velocity determination. **FIG 8** shows the residual median velocity of the Sun measured by the instrument after correcting for the Sun-spacecraft velocity for several days. The residual pattern has an amplitude of a few 10s of m/s that can be fit (see **FIG 9** for the time-dependent polynomial coefficients) and used as a second correction, but it winds up being a not-so-good extrapolation for high velocities. Clearly something about the filter profiles and instrument characteristics is not perfectly understood. **FIG 10** shows another interesting dependence of velocity on the roll angle of the instrument. Better understanding of the filters and their spatial and angular sensitivities is required.

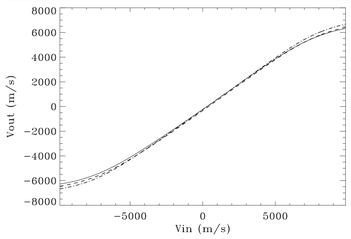

FIG 7: The curves show the velocity sensitivity table for each of several HMI calibration schemes in terms of the MDI-method output velocity as a function of the input solar velocity. The inverse lookup table is used to correct the velocity values.

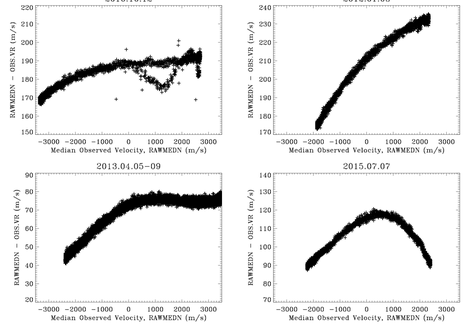

FIG 8: The top and right panels show the difference between the median solar velocity and the known Sun-SDO velocity as a function of observed velocity on several days. The lower left panel shows how the pattern drifts only slowly over 5 consecutive days. The upper left panel also shows what happens during a roll of the spacecraft.

Step 6 – The Vector Observables

The vector observables are the four Stokes parameters at each of the six HMI wavelengths averaged every 720s. They are more difficult to interpret, since the quantity of greatest interest is the vector magnetic field that depends on a complex inversion of the Stokes values. **FIG 11** shows how the inverted magnetic field depends on solar velocity for a stable sunspot. See caption for details. The LoS field component varies systematically by a few percent in strong field regions using both methods. The transverse component is independent of velocity, except for a curious excursion of +/- 5 G near 0 velocity in weak-field regions. In strong-field regions the MDI-like method depends on the magnitude of velocity rather than its signed value. **FIG 12** shows how the velocity-dependence of the MDI-like method depends on field strength. Between -750 and -1600 G the maximum daily difference in the measured LoS field strength increases from about 10 G to 25 G. **FIG 13** compares the observables determined with HMI tuned to four additional wavelengths. Using 10 wavelengths increases the reliability of the result, but cannot be done routinely.

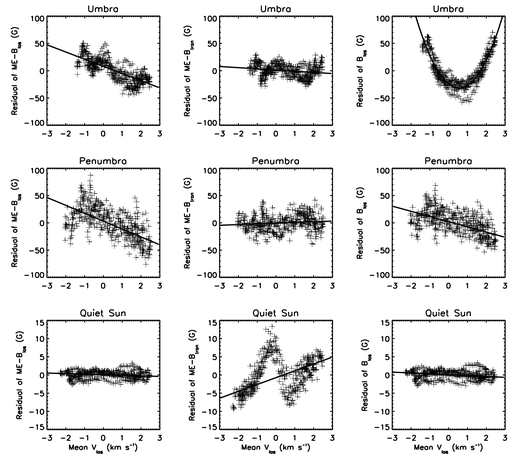

FIG 11: Each panel shows how a component of the measured magnetic field depends on Sun-SDO velocity in a stable sunspot region after the long-term trend has been removed. The top row is for umbra, the middle for penumbra, and the bottom for nearby quiet Sun. The left column is the line-of-sight component of the vector field. The right column is the line-of-sight component computed with the MDI-like method. The center column is the transverse component of the field. Note the scale is much smaller in the bottom row.

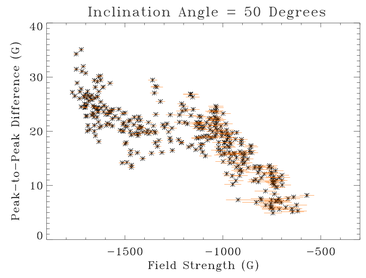

FIG 12: Using higher spectral resolution field strength determinations from the IBIS instrument as a reference, the figure shows how the maximum difference in LoS field strength determined by the MDI-like algorithm changes as a function of field strength. The daily difference is related to the +1860 to -2016 m/s velocity of the spacecraft.

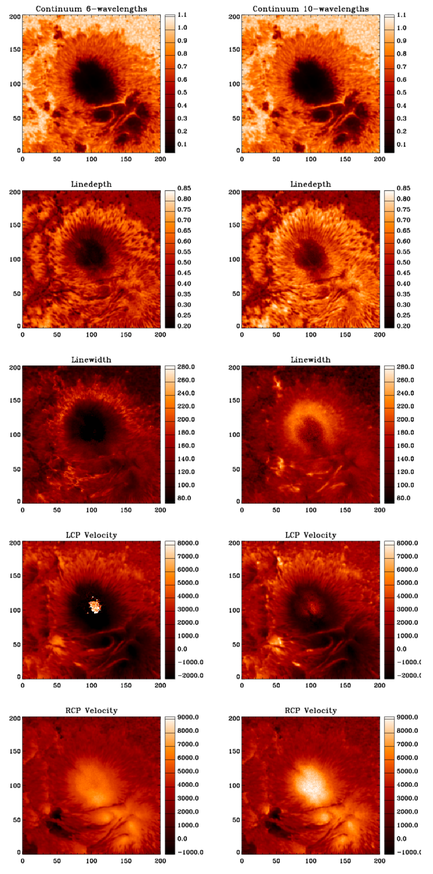

FIG 13: The left and right columns show the results of the LoS observables calculations based on HMI measurements of 6 and 10 different wavelengths taken on 24 Oct 2014.

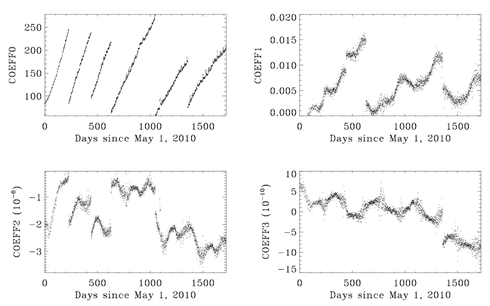

FIG 9: The coefficients of a third-order polynomial fit to the residual median velocity as a function of time. The constant term (upper left) drifts until a tuning change is made. The other coefficients show annual variations and jumps when the tuning and other changes are made to the instrument.

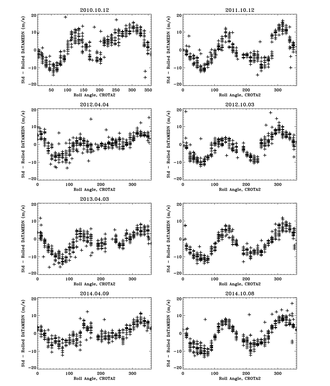

FIG 10: Each panel shows the change in median measured solar velocity as a function of roll angle on a day when the spacecraft was rolled. Differences are determined relative to nearby times when the Sun-SDO velocity was the same.

Step 7 –Additional Information Not Yet Used Routinely in Observables

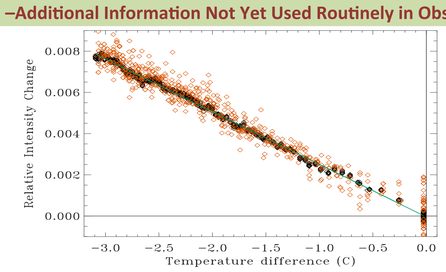

FIG 14: The intensity observables have not been intensively used or evaluated. There is a fairly small dependence of intensity on CCD temperature that has not been used to correct the intensities. The temperature typically varies by a couple K each day and the measurement decreases by a factor of 0.0025/K.

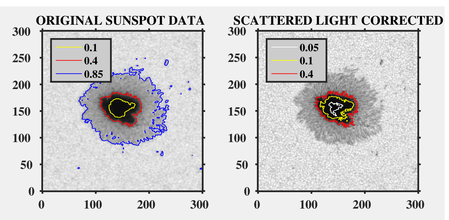

FIG 15: Scattered light can be corrected and various methods have been proposed to account for both small and large-scale sources of scattering. Our PSF correction relies on measured pre-launch characteristics of the optical path and on-orbit measurements of scattered light during eclipses, transits, and off points. The figure shows before and after images of a sunspot observed by HMI when scattered light is corrected. The dark core of the spot changes from 5.5% to 3.3% of the nearby quiet-Sun continuum and the granulation contracts increases from 3.7% to 7.2%.

Step 8 – CONCLUSION

The HMI instrument is well characterized and more than meets all of its original performance specifications. The data are more than adequate for achieving the original science goals of the project. Random errors are consistent with anticipated photon noise and instrument design parameters. However, systematic errors exist at the few percent level, attributable mainly to daily variations in the Sun-SDO velocity. The errors are reasonably well characterized and most sources are understood in principle. Continuing work is underway to improve the knowledge of the filter profiles that should reduce the errors. Empirical fixes for many issues can be implemented. In many cases reasonable accommodations can mitigate the remaining errors for many investigations. The HMI team is anxious to work with the community to improve the utility of the observations.